First Dark Matter Results from the XENON100 Experiment

E. Aprile,[1] K. Arisaka,[2] F. Arneodo,[3] A. Askin,[4] L. Baudis,[4] A. Behrens,[4] K. Bokeloh,[6] E. Brown,[2] J. M. R. Cardoso,[5] B. Choi,[1] D. B. Cline,[2] S. Fattori,[3] A. D. Ferella,[4] K.-L. Giboni,[1] A. Kish,[4] C. W. Lam,[2] J. Lamblin,[7] R. F. Lang,[1] K. E. Lim,[1] J. A. M. Lopes,[5] T. Marrodán Undagoitia,[4] Y. Mei,[8] A. J. Melgarejo Fernandez,[1] K. Ni,[9] U. Oberlack,[8] S. E. A. Orrigo,[5] E. Pantic,[2] G. Plante,[1,*] A. C. C. Ribeiro,[5] R. Santorelli,[4] J. M. F. dos Santos,[5] M. Schumann,[4,8] P. Shagin,[8] A. Teymourian,[2] D. Thers,[7] E. Tziaferi,[4] H. Wang,[2] and C. Weinheimer[6]

(XENON100 Collaboration)

[1]*Physics Department, Columbia University, New York, New York 10027, USA*
[2]*Physics & Astronomy Department, University of California, Los Angeles, USA*
[3]*INFN Laboratori Nazionali del Gran Sasso, Assergi, 67100, Italy*
[4]*Physics Institute, University of Zürich, Winterthurerstr. 190, CH-8057, Switzerland*
[5]*Department of Physics, University of Coimbra, R. Larga, 3004-516, Coimbra, Portugal*
[6]*Institut für Kernphysik, Westfälische Wilhelms-Universität Münster, 48149 Münster, Germany*
[7]*SUBATECH, Ecole des Mines de Nantes, Université de Nantes, CNRS/IN2P3, Nantes, France*
[8]*Department of Physics and Astronomy, Rice University, Houston, Texas 77005 - 1892, USA*
[9]*Department of Physics, Shanghai Jiao Tong University, Shanghai, 200240, China*

(Received 30 April 2010; revised manuscript received 7 June 2010; published 20 September 2010)

The XENON100 experiment, in operation at the Laboratori Nazionali del Gran Sasso in Italy, is designed to search for dark matter weakly interacting massive particles (WIMPs) scattering off 62 kg of liquid xenon in an ultralow background dual-phase time projection chamber. In this Letter, we present first dark matter results from the analysis of 11.17 live days of nonblind data, acquired in October and November 2009. In the selected fiducial target of 40 kg, and within the predefined signal region, we observe no events and hence exclude spin-independent WIMP-nucleon elastic scattering cross sections above 3.4×10^{-44} cm^2 for 55 GeV/c^2 WIMPs at 90% confidence level. Below 20 GeV/c^2, this result constrains the interpretation of the CoGeNT and DAMA signals as being due to spin-independent, elastic, light mass WIMP interactions.

DOI: 10.1103/PhysRevLett.105.131302 PACS numbers: 95.35.+d, 14.80.Ly, 29.40.−n, 95.55.Vj

A vast array of observational evidence suggests that 83% of the matter in the Universe is in some unknown form called dark matter [1]. Extensions of the standard model of particle physics that aim at addressing some of the puzzles associated with the electroweak scale predict stable weakly interacting massive particles (WIMPs), that can be thermally produced in the early Universe and become ideal dark matter candidates [2]. One method to detect WIMPs is to measure the energy they deposit in a detector by scattering off target nuclei.

XENON100 is a new ultralow background detector developed to continue the XENON dark matter search program with liquid xenon (LXe) as WIMP target and detection medium. Like XENON10 [3], it is a three-dimensional (3D) position-sensitive dual-phase (liquid-gas) time projection chamber (TPC) filled with ultrapure LXe. Particle interactions in the sensitive LXe volume are measured with two arrays of photomultiplier tubes (PMTs), which simultaneously detect the primary scintillation ($S1$) and the ionization signal ($S2$), via the proportional scintillation mechanism [4]. The 3D event localization allows "fiducialization" of the TPC, keeping only an inner volume in which the background rate is drastically reduced. The different ionization density of nuclear recoils, from neutrons or WIMPs, and electronic recoils, from γ or β backgrounds, leads to a different $S2/S1$ ratio, which can be used to discriminate the two types of recoils.

The detector uses 161 kg of LXe, divided in two concentric cylindrical volumes. These are physically and optically separated from each other by polytetrafluoroethylene (PTFE) panels on the side, a PMT array on the bottom, and a stainless steel diving bell on the top. The bell allows the inner liquid level to be set independently of the outer one. The PTFE panels define the TPC with 30.5 cm diameter and 30.6 cm height, acting also as an efficient UV reflector. Four stainless steel meshes provide the electric field to drift ionization electrons in the liquid, extract them to the gas phase, and accelerate them to produce proportional scintillation. A drift field of 530 V/cm has been used for the measurements reported here.

The PMTs are 2.5 cm $\times$ 2.5 cm metal-channel type (R8520-AL) specifically developed in collaboration with Hamamatsu Co. for operation in LXe, with a quantum

efficiency of about 30% at 178 nm and with low intrinsic radioactivity (1 mBq/PMT in ^{238}U/^{232}Th). The 80 PMT array at the bottom of the TPC is immersed in the liquid to efficiently detect the $S1$ signal, while another array of 98 PMTs is placed in the xenon gas above the anode so that the hit pattern of an $S2$ signal can be used to reconstruct the event position in (x, y). The interaction depth (z) in the detector can be computed from the time difference between $S1$ and $S2$ pulses with resolution <2 mm. The outermost LXe volume is used as an active veto, instrumented with 64 PMTs. The energy threshold of the veto has been measured to be better than 200 keV$_{ee}$ (keV electron equivalent [5] as inferred from ^{137}Cs). The signals from all 242 PMTs are digitized at 100 MS/s and 40 MHz bandwidth. The trigger is provided by the summed signal of 84 central PMTs, low-pass filtered with 1 MHz. Given the strong amplification in the gas proportional region, at low energies the trigger is given by the $S2$ pulse, with an efficiency $>99\%$ above 300 photoelectrons (PE).

The detector has been deployed underground at the Laboratori Nazionali del Gran Sasso (LNGS), where the muon flux is reduced by a factor 10^6, thanks to the average 3600 m water equivalent of rock overburden. The LXe is contained in a double walled, vacuum insulated, stainless steel cryostat. A 200 W pulse tube refrigerator (PTR) continuously liquefies the gas circulated through a hot getter and maintains the liquid at -91 °C. The PTR system is installed outside a passive shield to achieve a lower radioactive background in the target. This shield consists of a 20 cm thick layer of lead and a 20 cm thick layer of polyethylene within, to attenuate the background from external γ rays and neutrons, respectively. The shield structure rests on a 25 cm thick slab of polyethylene and is surrounded on the top and three sides by a 20 cm thick water layer to lower the background contribution from neutrons from the cavern rock. A 5 cm thick layer of copper covers the inner surface of the polyethylene to attenuate the gamma background due to its radioactivity. Calibration sources (^{57}Co, ^{60}Co, ^{137}Cs, ^{241}AmBe) are inserted through a copper tube which penetrates the shield and circles around the detector in the middle of the drift region.

The gas used in XENON100 has been processed through a distillation column to reduce the ^{85}Kr background to 33 μBq/kg, as measured with delayed $\beta-\gamma$ coincidences [6]. Assuming an isotopic abundance of 10^{-11}, this ^{85}Kr contamination corresponds to 143^{+130}_{-90} ppt (mol/mol), at 90% confidence, of natural Kr.

PMT gains are measured under single PE conditions using light emitting diodes (LEDs) coupled to optical fibers which illuminate the TPC and veto volumes. The PMT gains, equalized to 1.9×10^6 at the beginning of the run, are regularly monitored and are stable within $\pm2\%$ (σ/μ).

Event positions are calculated using three independent algorithms, based on χ^2 minimization, support vector machine regression, and a neural network. We take the PMT gains into account and correct for nonuniformities of the drift field as inferred from a finite element simulation. The three algorithms give consistent results for radii $r<14$ cm with an (x, y) resolution better than 3 mm, as measured with a collimated γ source. This motivated the choice, for the present analysis, of a 40 kg fiducial volume as a cylinder of radius 13.5 cm and height 24.3 cm.

Corrections for the spatial dependence of the $S1$ light collection in the TPC are obtained by irradiating the detector at different azimuthal positions with an external ^{137}Cs source and computing the average light yield in 1 cm $\times$ 2.5 cm (r, z) cells. The average light yield of the whole TPC for ^{137}Cs 662 keV$_{ee}$ γ rays is 1.57 PE/keV$_{ee}$ at a field of 530 V/cm. The spatial correction is also inferred using 40 keV$_{ee}$ γ rays produced via the inelastic reaction ^{129}Xe$(n, n'\gamma)^{129}$Xe, together with 80 keV$_{ee}$ γ rays from ^{131}Xe$(n, n'\gamma)^{131}$Xe, during the calibration of the detector with an external ^{241}AmBe source. These γ rays are more uniformly distributed in the sensitive volume due to the larger neutron mean free path. In addition, 164 keV$_{ee}$ and 236 keV$_{ee}$ γ rays are produced following the same neutron calibration from the decay of metastable ^{131m}Xe and ^{129m}Xe, respectively. The 164 keV$_{ee}$ line is also used to infer the $S1$ spatial dependence. The corrections inferred from these independent calibrations differ by less than 3% and improve the energy resolution (σ/E) at 662 keV$_{ee}$ from 24% to 13% using the scintillation signal alone.

Calibrations with ^{137}Cs were taken daily during the data taking presented here, to infer the electron lifetime and to subsequently correct the $S2$ signal for its drift time dependence. The electron lifetime increased from 154 μs to 192 μs, resulting in the average $S2$ z correction decreasing from 75% to 60%. The $S2$ signal is also corrected for its (x, y) variation, mostly due to light collection effects near the edge of the TPC. This dependence is determined using the 40 keV$_{ee}$ γ rays from the neutron calibration data and computing the proportional scintillation light yield in 2 cm $\times$ 2 cm (x, y) cells. Only insignificant differences ($<2\%$) were observed between corrections obtained using other calibration data sets of various γ-ray energies (164 keV$_{ee}$, 662 keV$_{ee}$). The energy resolution (σ/E) at 662 keV$_{ee}$ using the $S2$ signal alone is improved from 7.3% to 6.5% after applying the $S2$ spatial corrections.

The nuclear-recoil equivalent energy E_{nr} in LXe is conventionally computed from the scintillation signal, $S1$, using $E_{nr}=(S1/L_y)(1/\mathcal{L}_{eff})(S_{ee}/S_{nr})$, where $\mathcal{L}_{eff}$ is the scintillation efficiency of nuclear recoils relative to that of 122 keV$_{ee}$ γ rays at zero field, and S_{ee} and S_{nr} are the electric field scintillation quenching factors for electronic and nuclear recoils, respectively, with measured values of 0.58 and 0.95 [7]. Since 122 keV$_{ee}$ γ rays cannot penetrate far in the sensitive volume, their light yield L_y at 530 V/cm is calculated from a fit to all γ-ray lines men-

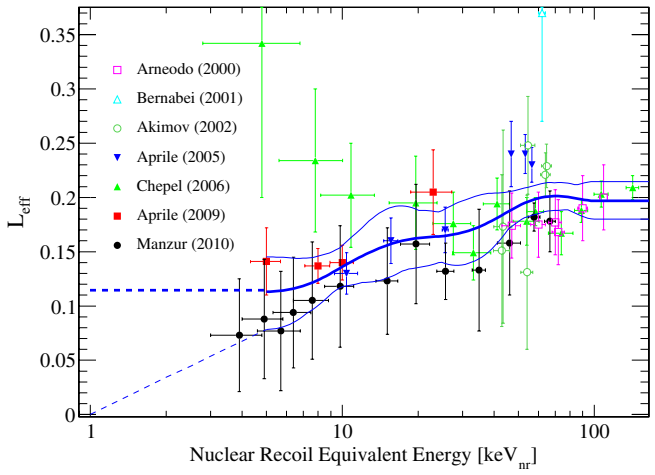

FIG. 1 (color online). Global fit to all $\mathcal{L}_{\rm eff}$ measurements with fixed neutron energies between 5 keV$_{\rm nr}$ and 100 keV$_{\rm nr}$, together with 90% confidence contours (solid lines) and extrapolations to lower energies (dashed lines).

tioned above, yielding $L_y(122\ \text{keV}_{\rm ee}) = (2.20 \pm 0.09)$ PE/keV$_{\rm ee}$. $\mathcal{L}_{\rm eff}$ data measured at fixed neutron energies [5,8,9], shown in Fig. 1, have less systematic uncertainty than those inferred from a comparison of neutron calibration spectra with Monte Carlo simulations. Therefore, the energy dependence of $\mathcal{L}_{\rm eff}$ and its uncertainty is determined here through a global cubic-spline fit to all data shown in Fig. 1 in the energy range with at least two measurements (5–100 keV$_{\rm nr}$). The spline knots are fixed at 5, 10, 25, 50, and 100 keV$_{\rm nr}$. Below 5 keV$_{\rm nr}$, a constant extrapolation of the global fit, consistent with the trend reported in Aprile *et al.* [5] and Sorensen *et al.* [10], is used in this analysis. A logarithmic extrapolation of the lower 90% confidence contour to zero scintillation near 1 keV$_{\rm nr}$, following the trend in Manzur *et al.* [8], is also shown in Fig. 1.

Data selection criteria are motivated by the physical properties of xenon scintillation light, the characteristics of proportional light signals, and the expected WIMP-induced single-scatter nuclear-recoil signature. Cuts were developed and tested on calibration data, specifically on low energy electronic recoils from Compton scattered ^{60}Co γ rays and nuclear recoils from ^{241}AmBe. In particular, a twofold PMT coincidence is required in a 20 ns window for the $S1$ signal and events which contain more than a single $S1$-like pulse are discarded. This allows true low energy events to be distinguished from events with random single photoelectrons from PMTs or accidental coincidences. For the $S2$ signal, a lower threshold of 300 PE is set, corresponding to about 15 ionization electrons, and events are required to contain only one $S2$ pulse above this threshold. This rejects events with multiple scatters at different z positions. In addition, the width of the $S2$ pulse is required to be consistent with what is expected from the inferred drift time due to diffusion of the electron cloud [11].

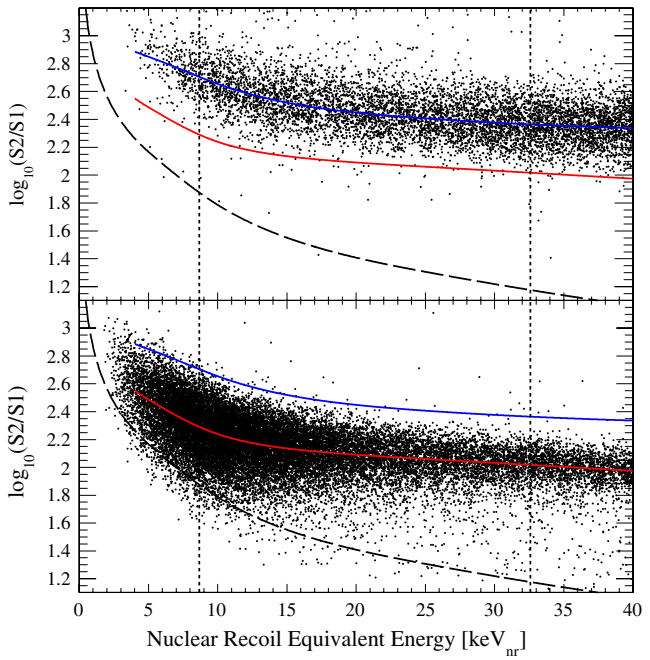

FIG. 2 (color online). Electronic (top) and nuclear (bottom) recoil bands from ^{60}Co and ^{241}AmBe calibration data, respectively, after data selection and the 40 kg fiducial volume cut. Colored lines correspond to the median $\log_{10}(S2/S1)$ values of the electronic (blue [dark grey]) and nuclear (red [light grey]) recoil bands. The WIMP search energy window 8.7–32.6 keV$_{\rm nr}$ (vertical, dashed line) and $S2$ software threshold of 300 PE (long dashed line) are shown.

Events that deposit energy in the veto volume in coincidence with the $S1$ signal in the TPC are also discarded. The regions of the digitized waveform away from $S1$ or $S2$ pulses are required to be free of extraneous PMT signals or noise. Finally, events outside the predefined fiducial volume are rejected.

Background rejection in XENON100 is achieved through a combination of volume fiducialization and the identification of recoil species based on the ratio $S2/S1$ for electronic and nuclear recoils. Accurate knowledge of the response to both types of recoils is essential to define the signal region, to determine the signal acceptance, and to predict the expected leakage into the signal region. Statistics for the low energy electronic recoil calibration are accumulated at regular intervals with a 1 kBq ^{60}Co source. The response of XENON100 to elastic nuclear recoils was obtained by irradiating the detector with a 220 n/s ^{241}AmBe source for 72 h. Figure 2 shows the $\log_{10}(S2/S1)$ distribution of single-scatter electronic and nuclear recoils in the 40 kg fiducial volume, as function of nuclear-recoil energy. The energy window for the WIMP search is chosen between 8.7–32.6 keV$_{\rm nr}$ (4–20 PE). The upper bound is taken to correspond approximately to the one used for the XENON10 blind analysis [3], after recomputing the corresponding nuclear-recoil equivalent energy using the new $\mathcal{L}_{\rm eff}$ parametrization from the global fit,

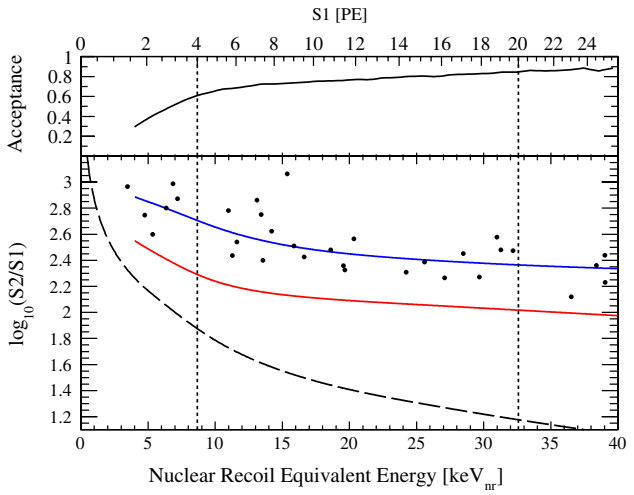

FIG. 3 (color online). Cut acceptance (top, not including 50% acceptance from $S2/S1$ discrimination) and $\log_{10}(S2/S1)$ (bottom) as functions of nuclear-recoil energy for events observed in the 40 kg fiducial volume during 11.17 live days. Lines as in Fig. 2.

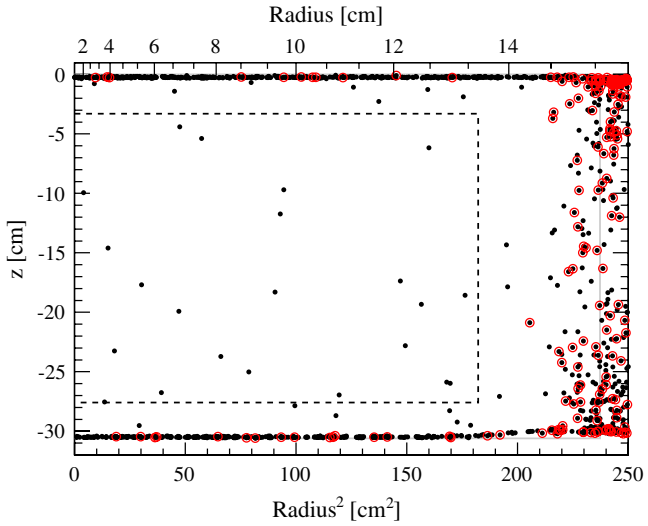

FIG. 4 (color online). Distribution of all events (dots) and events below the nuclear-recoil median (red circles) in the TPC (grey line) observed in the 8.7–32.6 $\mathrm{keV_{nr}}$ energy range during 11.17 live days. No events below the nuclear-recoil median are observed within the 40 kg fiducial volume (dashed line).

shown in Fig. 1. The lower bound is motivated by the fact that the acceptance of the $S1$ twofold coincidence requirement is >90% above 4 PE. The $\log_{10}(S2/S1)$ upper and lower bounds of the signal region are, respectively, chosen as the median of the nuclear-recoil band and the 300 PE $S2$ software threshold.

A first dark matter analysis has been carried out, using 11.17 live days of background data, taken from October 20th to November 12th 2009, prior to the neutron calibration. Although this was not formally a blind analysis, all the event selection criteria were optimized based on calibration data only. The cumulative software cut acceptance for single-scatter nuclear recoils is conservatively estimated to vary between 60% (at 8.7 $\mathrm{keV_{nr}}$) and 85% (at 32.6 $\mathrm{keV_{nr}}$) by considering all single-scatter events in the fiducial volume that are removed by only a single cut to be valid events (Fig. 3). Visual inspection of hundreds of events confirmed that this is indeed a conservative estimate. Within the 8.7–32.6 $\mathrm{keV_{nr}}$ energy window, 22 events are observed, but none in the predefined signal acceptance region (Fig. 3). At 50% nuclear-recoil acceptance, the electronic recoil discrimination based on $\log_{10}(S2/S1)$ is above 99%, predicting <0.2 background events in the WIMP region. The observed rate, spectrum, and spatial distribution (Fig. 4) agree well with a GEANT4 Monte Carlo simulation of the entire detector.

An upper limit on the spin-independent WIMP-nucleon elastic scattering cross section is derived based on the assumption of an isothermal WIMP halo with $v_0 = 220$ km/s, density 0.3 GeV/c^2, and escape velocity 544 km/s [12]. We take a $S1$ resolution dominated by Poisson fluctuations into account and use the global fit $\mathcal{L}_{\mathrm{eff}}$ with constant extrapolation below 5 $\mathrm{keV_{nr}}$. The acceptance-corrected exposure in the energy range considered, weighted by the spectrum of a 100 GeV/c^2 WIMP, is 172 kg · days. Figure 5 shows the resulting 90% confidence upper limit, with a minimum at a cross section of 3.4×10^{-44} $\mathrm{cm^2}$ for a WIMP mass of 55 GeV/c^2. The impact of assuming the lower 90% confidence $\mathcal{L}_{\mathrm{eff}}$ contour together with the extrapolation to zero around 1 $\mathrm{keV_{nr}}$ is also shown. Our limit constrains the interpretation of the

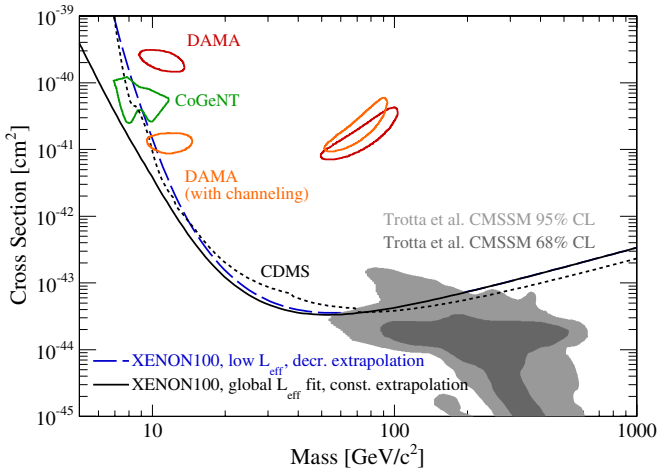

FIG. 5 (color online). 90% confidence limit on the spin-independent elastic WIMP-nucleon cross section (solid and long dashed lines), together with the best limit to date from CDMS (dotted line) [15], recalculated assuming an escape velocity of 544 km/s and $v_0 = 220$ km/s. Expectations from a theoretical model [16], and the areas (90% C.L.) favored by CoGeNT (green) [13] and DAMA (red/orange) [14] are also shown.

CoGeNT [13] and DAMA [14] signals as being due to light mass WIMPs. These initial results, based on only 11.17 live days of data, demonstrate the potential of the XENON100 low-background experiment to discover WIMP dark matter.

We gratefully acknowledge support from NSF, DOE, SNF, the Volkswagen Foundation, FCT, and STCSM. We are grateful to the LNGS for hosting and supporting the XENON program. We acknowledge the contributions of T. Bruch (UZH), K. Lung (UCLA), A. Manalaysay (UZH), and M. Yamashita (U. Tokyo).

*guillaume.plante@astro.columbia.edu

[1] E. Komatsu *et al.*, Astrophys. J. Suppl. Ser. **180**, 330 (2009).
[2] G. Bertone, D. Hooper, and J. Silk, Phys. Rep. **405**, 279 (2005).
[3] J. Angle *et al.*, Phys. Rev. Lett. **100**, 021303 (2008).
[4] A. Lansiart *et al.*, Nucl. Instrum. Methods **135**, 47 (1976).
[5] E. Aprile *et al.*, Phys. Rev. C **79**, 045807 (2009).
[6] E. Aprile *et al.*, arXiv:1001.2834.
[7] E. Aprile *et al.*, Phys. Rev. Lett. **97**, 081302 (2006).
[8] A. Manzur *et al.*, Phys. Rev. C **81**, 025808 (2010).
[9] F. Arneodo *et al.*, Nucl. Instrum. Methods Phys. Res., Sect. A **449**, 147 (2000); R. Bernabei *et al.*, Eur. Phys. J. direct C **11**, 1 (2001); D. Akimov *et al.*, Phys. Lett. B **524**, 245 (2002); E. Aprile *et al.*, Phys. Rev. D **72**, 072006 (2005); V. Chepel *et al.*, Astropart. Phys. **26**, 58 (2006).
[10] P. Sorensen *et al.*, Nucl. Instrum. Methods Phys. Res., Sect. A **601**, 339 (2009).
[11] T. Doke, Nucl. Instrum. Methods **196**, 87 (1982).
[12] J. D. Lewin and P. F. Smith, Astropart. Phys. **6**, 87 (1996); M. C. Smith *et al.*, Mon. Not. R. Astron. Soc. **379**, 755 (2007).
[13] C. E. Aalseth *et al.*, arXiv:1002.4703.
[14] C. Savage *et al.*, J. Cosmol. Astropart. Phys. 04 (2009) 010.
[15] Z. Ahmed *et al.*, Science **327**, 1619 (2010).
[16] R. Trotta *et al.*, J. High Energy Phys. 12 (2008) 024.